

## Particle creation in left-handed metamaterial transmission lines

Alessandro Ferreri <sup>1,\*</sup>, David Edward Bruschi <sup>1,2</sup> and Frank K. Wilhelm <sup>1,2</sup>

<sup>1</sup>*Institute for Quantum Computing Analytics (PGI-12), Forschungszentrum Jülich, 52425 Jülich, Germany*

<sup>2</sup>*Theoretical Physics, Universität des Saarlandes, 66123 Saarbrücken, Germany*



(Received 27 February 2024; accepted 6 August 2024; published 22 August 2024)

Transmission lines (TLs) are excellent examples of quantum simulators of quantum fields. By appropriately driving-specific circuit elements, these devices can reproduce relativistic and quantum phenomena such as particle creation due to the nonadiabatic stimulation of the quantum vacuum. We investigate particle creation in left-handed TLs induced by the modulation of the Josephson energy in superconducting quantum interference devices. Our results show that, as a consequence of the peculiar dispersion relations present in these systems, particle production occurs with much more favorable conditions with respect to the usual right-handed TLs.

DOI: [10.1103/PhysRevResearch.6.033204](https://doi.org/10.1103/PhysRevResearch.6.033204)

### I. INTRODUCTION

Quantum field theory in flat [1] and curved [2–4] spacetime is the best available mathematical apparatus that underpins our comprehension of relativistic and quantum many-body phenomena. Among its most successful predictions, one finds highly energetic processes such as the dynamical Casimir effect (DCE) [5–8], the Unruh effect [9–12], and Hawking radiation [13–15]. Unfortunately, due to the considerable energy scales and the extreme conditions necessary to witness such phenomena, their direct observation has not been possible to date. Nevertheless, in the last decade, impressive advancements in quantum technologies based on quantum simulation platforms have led to the successful fabrication of devices that mimic well the main features of such highly energetic phenomena [16–21].

Quantum simulators are powerful tools for the study of quantum processes whose reproduction and control in the laboratory is, in many cases, unfeasible [22,23]. Among the vast range of possible quantum simulating devices, here, we want to focus our attention on one specific class, which can describe well the dynamics of quantum fields in nonadiabatic scenarios, namely, superconducting circuits based on transmission lines (TLs) [24–29]. In the frameworks of quantum field theory and cosmology, these platforms find many theoretical and experimental applications in the engineering of space-time analogs [21,30,31] as well as the simulation of particle creation phenomena [32–34], such as the DCE [35–37] and Hawking radiation [38–40].

In general, the dynamics of quantum scalar fields and particle creation phenomena are always described in an environment characterized by a positive dielectric constant

and magnetic permeability. However, in the last decades, particular dedication has been made to theoretically and experimentally engineering metamaterials characterized by left-handed dispersion relations [41–43]. In left-handed metamaterials, the phase velocity has the opposite sign with respect to the Poynting vector, which stems from the fact that both the dielectric constant and the magnetic permeability of the medium are negative [44].

In one-dimensional systems, such as TLs, the left-handedness emerges when the dispersion law displays a negative group velocity. A standard left-handed TL (LHTL), such as that depicted in Fig. 1(a), can be assembled starting from the model of a right-handed TL (RHTL) by interchanging capacitors and inductors [45] [see also Fig. 2(a)]. As a consequence, LHTLs can be seen as duals of RHTLs [46,47]. Among other uses, LHTLs and hybrid platforms can find applications in circuit quantum electrodynamics for the simulations of multimode quantum systems [47–51].

We propose two platforms based on LHTLs, whose dynamics is regulated by a set of superconducting quantum interference devices (SQUIDs) [52,53]. The difference between the two schemes relies on the placement of the SQUID, which leads to two different spectra. As first, we show that the proper quantization of LHTLs leads to unusual commutation relations of the bosonic ladder operators. Indeed, unlike standard RHTLs, the commutator between the annihilation and the creation operators in LHTLs explicitly depends on the mode wave vector. We will see that this has astonishing consequences on the time evolution of the ladder operators. We will explore the dynamics of such TLs by studying the dynamics of the quantum magnetic flux  $\hat{\Phi}$ , showing that we can stimulate the quantum vacuum of the TL and generate pairs of bosonic excitations. Interestingly, we can attribute a different physical interpretation to the particle production depending on the placement of the circuit elements.

This paper is structured as follows: In Sec. II, we introduce the two LHTLs and calculate the dispersion relations starting from the linear Lagrangians of the circuits. In Sec. III, we present the protocols to quantize the magnetic flux field along the two TLs. In Sec. IV, we show our main results: The nona-

\*Contact author: a.ferreri@fz-juelich.de

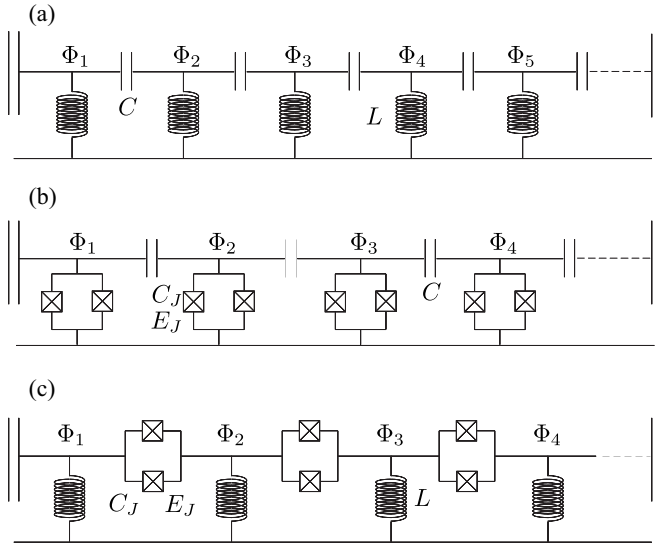


FIG. 1. Schematic representations of the left-handed transmission line (LHTL). (a) Standard LHTL. (b) Circuit 1: LHTL with a set of superconducting quantum interference devices (SQUIDs) in parallel. (c) Circuit 2: LHTL with a set of SQUIDs in series.

adiabatic modulation of the Josephson energy at the SQUIDs stimulates the creation of bosons along the TL. Finally, in Appendix A, we briefly discuss standard RHTLs present in the literature, while in Appendixes B and C, we present details about calculations, with particular focus on the input-output formalism and the multiscale analysis.

## II. CLASSICAL LHTLS

We introduce three LHTLs based on the presence or absence of capacitors and inductors: We refer to Fig. 1(a) as a *standard scheme*, to Fig. 1(b) as *circuit 1*, and to Fig. 1(c) as *circuit 2*. The difference between the last two platforms relies on the placement of the SQUID: Circuit 1 is characterized by a set of SQUIDs placed in parallel, whereas in circuit 2, all SQUIDs are placed in a series. Each circuit consists of  $N$  cells; each thereof has length  $\Delta x$ .

We assume that each SQUID is characterized by the capacitance  $C_J$ , the Josephson energy  $E(t)$ , and the phase  $\varphi = 2\pi\Phi_J/\phi_0$ , where  $\Phi_J$  is the magnetic flux at the SQUID, and  $\phi_0 = \pi\hbar/e$  is the magnetic flux quantum. Importantly, we will assume small amplitude of the plasma oscillation in the SQUID, i.e.,  $\Phi_J/\phi_0 \ll 1$ , and that all SQUIDs work in the phase regime  $E(t) \gg (2e)^2/2C_J$  [36,54], thereby expanding the Josephson energy at the lowest order in  $\Phi_J/\phi_0$  [55]. Finally, we make the identification  $\Phi_J = \Phi$ , where  $\Phi$  is the magnetic flux on the TL [37,54].

The Josephson energy can be externally driven to have a time-dependent dispersion relation. In each platform discussed in this paper, we will modulate the Josephson energy via  $E(t) = E_0[1 + 4\eta \sin(\Omega t)]$  around the constant value  $E_0 = I_c\phi_0$  [5], where  $I_c$  is critical current,  $\Omega$  is the oscillation frequency, and  $\eta \ll 1$  is dimensionless oscillation amplitude.

Note that, in contrast with any right-handed platforms discussed in the literature (see, for instance, Refs. [33,34]), the mathematical description of LHTLs must account for the

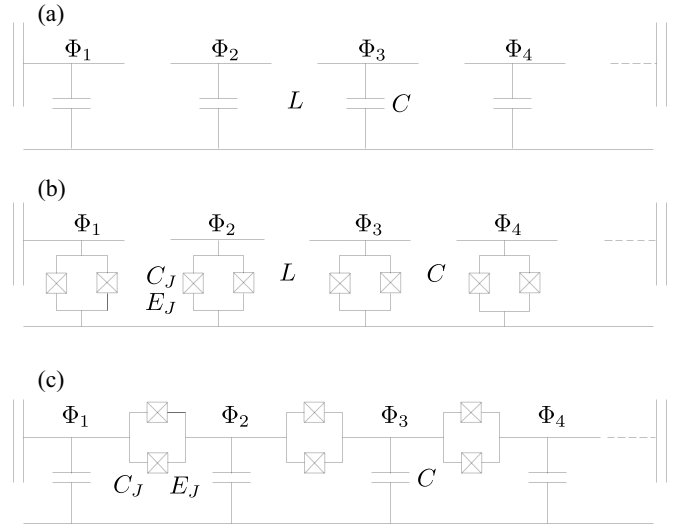


FIG. 2. Schematic representations of the right-handed transmission line (RHTL). (a) Standard RHTL. (b) Circuit 1: RHTL with a set of superconducting quantum interference devices (SQUIDs) in parallel. (c) Circuit 2: RHTL with a set of SQUIDs in series.

infrared bound of the dispersion relations [47], as we will discuss later. Therefore, we cannot describe the space along the TL in the continuous limit  $\Delta x \rightarrow 0$ , as normally accomplished for RHTL, since this would cause the divergence of the frequency at long wavelengths.

### A. Circuit 1: SQUIDs in parallel

As a first case, we want to study the LHTL pictorially represented in Fig. 1(b). At each node, we replace the inductors of the standard LHTL shown in Fig. 1(a) with a SQUID having capacitance and Josephson energy  $C_J$  and  $E_J = E(t)$ , respectively, whereas a capacitor with capacitance  $C$  is placed between two nodes.

In the linearized limit of the SQUID [37,54], the Lagrangian of the system expressed in terms of the magnetic flux is

$$\mathcal{L} = \frac{1}{2} \sum_{n=1}^N \left[ C(\dot{\Phi}_n - \dot{\Phi}_{n+1})^2 + C_J \dot{\Phi}_n^2 - \tilde{E}(t) \Phi_n^2 \right], \quad (1)$$

where  $\Phi_n$  indicates the magnetic flux field at node  $n$ , and  $\tilde{E}(t) = (2\pi/\phi_0)^2 E(t)$ .

To describe the dynamics of the TL, we need to solve the equations of motion obtained via the Euler-Lagrange equations  $\frac{d}{dt} \partial \mathcal{L} / \partial \dot{\Phi}_n - \partial \mathcal{L} / \partial \Phi_n = 0$ . These equations admit a set of solutions of the form  $\exp(i n \Delta x k - i \omega t)$ . We then compute the dispersion relation of the TL and obtain

$$\omega_j(t) = \sqrt{\frac{\tilde{E}(t)}{4C \sin^2\left(\frac{k_j \Delta x}{2}\right) + C_J}}, \quad (2)$$

where the wave vector  $k_j = \frac{2\pi j}{N \Delta x}$  is bounded within the first Brillouin zone  $j = \pm 1, \dots, \pm N/2$  [47]. The left-handedness of the TL clearly emerges from the group velocity defined as  $v_g = \partial \omega / \partial k$ , which is negative. We note that the infrared limit of the TL is  $\omega_{\text{IR}} = \sqrt{\tilde{E}/(4C + C_J)} \simeq \sqrt{\tilde{E}/4C}$ , which

is reached at the border of the first Brillouin zone, where  $k_{N/2} = \pi/\Delta x$ , and is valid when  $4C \gg C_J$  [47].

### B. Circuit 2: SQUID in series

The second scheme we want to analyze is illustrated in Fig. 1(c). In this scheme, we replaced each capacitor of the standard LH TL in Fig. 1(a) with a SQUID having capacitance  $C_J$  and Josephson energy  $E(t)$ . The Lagrangian of the TL in the linearized limit of the SQUID is

$$\mathcal{L} = \frac{1}{2} \sum_{n=1}^N \left[ C(\dot{\Phi}_{n+1} - \dot{\Phi}_n)^2 - \frac{\Phi_n^2}{L} - \tilde{E}(t)(\Phi_{n+1} - \Phi_n)^2 \right], \quad (3)$$

where we made the identification  $C \equiv C_J$ , and  $L$  is the inductance. Assuming as before a solution of the equations of motion of the form  $\exp(in\Delta x k - i\omega t)$ , we find the following dispersion relation:

$$\omega_j(t) = \sqrt{\frac{1}{4CL \sin^2\left(\frac{k_j \Delta x}{2}\right)} + \frac{\tilde{E}(t)}{C}}, \quad (4)$$

where again the wave vector is  $k_j = \frac{2\pi j}{N\Delta x}$ , with  $j = \pm 1, \dots, \pm N/2$ .

Note that this dispersion relation structurally differs from Eq. (2), and in fact, it describes a different left-handed quantum field. Indeed, the frequencies in Eq. (4) consist of two parts: The first term inside the square root gives the standard relation between the frequency and wave vector in LH TLs; the second term does not depend on the wave vector, and it is identical for each mode. In field theory, the presence of the latter is the signature of a massive field [1]. Therefore, once we quantize the magnetic field flux, its excitations will behave as massive particles with a left-handed group velocity and time-dependent quadratic mass  $M^2(t) \propto \tilde{E}(t)/C$ . Note that, in contrast with the standard (right-handed) dispersion relation of the Klein-Gordon field wherein the massive term of the field becomes negligible in the ultrarelativistic limit ( $k \gg Mc/\hbar$ , with  $c$  speed of light), in this LH TL, the massive term becomes negligible in long-wavelength modes where  $k_j^2 \ll 1/[(\Delta x)^2 CL \tilde{E}(t)]$ .

### III. QUANTIZATION PROCEDURE

In this section, we discuss the formalism employed for the quantization of the two LH TLs presented in this paper, starting from basic circuit equations. Our goal is to achieve a quantized expression of both modes of the quantum magnetic flux fields and the Hamiltonian at  $t < 0$ , namely, before the beginning of the modulation of the Josephson energy. For this reason, we conveniently omit the time-dependence in the Josephson energy and write  $\tilde{E} = E_0(2\pi/\phi_0)^2$ .

As a first step, we solve the equations of motion of the two TLs. These can be achieved from the two Lagrangians in Eqs. (1) and (3), respectively, for circuits 1 and 2, by means

of the Euler-Lagrange equations. At any node  $1 < n < N$ , the equations of motion become

$$\ddot{\Phi}_{n+1} + \ddot{\Phi}_{n-1} - 2\ddot{\Phi}_n - \frac{C_J}{C} \ddot{\Phi}_n = \frac{\tilde{E}}{C} \Phi_n, \quad (5)$$

$$\ddot{\Phi}_{n+1} + \ddot{\Phi}_{n-1} - 2\ddot{\Phi}_n = \frac{\Phi_n}{CL} + \frac{\tilde{E}}{C}(2\Phi_n - \Phi_{n+1} - \Phi_{n-1}), \quad (6)$$

for circuits 1 and 2, respectively. In Eq. (6), we made the identification  $C_J \equiv C$ . Assuming plane-wave solution of the form  $\exp(in\Delta x k - i\omega t)$ , the magnetic flux is described by the expression:

$$\Phi(n, t) = \sum_{|j|=1}^{N/2} [\phi_j(n, t)a_j + \phi_j^*(n, t)a_j^*], \quad (7)$$

where the modes are defined by  $\phi_j(n, t \leq 0) = \sqrt{\frac{\hbar}{2CN\omega_{0j}}} \exp[i(k_j n \Delta x - \omega_{0j} t)]$ , and  $\omega_{0j} \equiv \omega_j(t \leq 0)$  are the mode frequencies [these will correspond to either Eq. (2) or (4) depending on the considered scheme]. Note that, since the minimum distinguishable wavelength is  $\lambda_{\min} = 2\Delta x$  [47], the sum over all modes runs up to  $N/2$ . The modes are normalized via the relation:

$$-\frac{iC}{\hbar} \sum_{n=1}^N \left[ \phi_i(n, t) \frac{\partial \phi_j^*(n, t)}{\partial t} - \frac{\partial \phi_i^*(n, t)}{\partial t} \phi_j(n, t) \right] = \delta_{ij}, \quad (8)$$

where we made use of the representation of the Kronecker delta  $\delta_{lh} = \frac{1}{N} \sum_{n=1}^N \exp[2\pi in(l-h)/N]$ .

The Hamiltonian of the TLs is achieved from the Lagrangian by means of the Legendre transformation  $\mathcal{H} = \sum_n [P_n \dot{\Phi}_n - \mathcal{L}]$ , with conjugated momenta:

$$P_n = \frac{\partial \mathcal{L}}{\partial \dot{\Phi}_n} = C(2\dot{\Phi}_n - \dot{\Phi}_{n+1} - \dot{\Phi}_{n-1}) + C_J \dot{\Phi}_n, \\ P_n = \frac{\partial \mathcal{L}}{\partial \dot{\Phi}_n} = C(2\dot{\Phi}_n - \dot{\Phi}_{n+1} - \dot{\Phi}_{n-1}), \quad (9)$$

for circuits 1 and 2, respectively.

We take advantage of both the mode expansion in Eq. (7) and the definition of the conjugate momentum in Eq. (9) to perform the discrete Fourier transform of both the field and the conjugate momentum, thereby obtaining the classical amplitude of the field in terms of  $\Phi_n$  and  $P_n$ . This reads

$$a_h = \zeta_h \sum_n^N \exp[-i(k_h n \Delta x - \omega_h t)] \\ \times \left[ \Phi(n, t) + \frac{i\chi_h^{-1}}{\omega_h} P(n, t) \right], \quad (10)$$

with  $\zeta_h = \sqrt{\frac{\omega_h C}{2\hbar N}}$ . The parameter  $\chi_h$  strictly depends on the scheme we are considering. It has the expression:

$$\chi_h = \begin{cases} 4 \sin^2\left(\frac{k_h \Delta x}{2}\right) + \frac{C_J}{C} & \text{for circuit 1,} \\ 4 \sin^2\left(\frac{k_h \Delta x}{2}\right) & \text{for circuit 2.} \end{cases}$$

The quantization of field and the canonical momentum are accomplished by imposing the equal time commutators  $[\hat{\Phi}(n, t), \hat{P}(m, t)] = i\hbar\delta_{nm}$  and  $[\hat{\Phi}(n, t), \hat{\Phi}(m, t)] = [\hat{P}(n, t), \hat{P}(m, t)] = 0$ . We then use these commutators, together with Eq. (10) and the discrete representation of the Kronecker delta provided before, to obtain the commutation relation of the quantized amplitude, promoted to annihilation and creation operators:

$$[\hat{a}_j, \hat{a}_h^\dagger] = \chi_j^{-1} \delta_{jh}. \quad (11)$$

The presence of the factor  $\chi_j$  in the denominator is key, as can be seen below.

We can now express the Hamiltonian  $\hat{\mathcal{H}}$  in terms of the ladder operators. By substituting the mode decomposition in Eq. (7), exploiting the normalization condition in Eq. (8), and taking advantage of the commutation rule in Eq. (11), the Hamiltonian reduces to

$$\hat{\mathcal{H}} = \hbar \sum_{|j|=1}^{N/2} \omega_{0j} \left[ \chi_j \hat{a}_j^\dagger \hat{a}_j + \frac{1}{2} \right]. \quad (12)$$

Note that the commutation relation in Eq. (11) preserves the correspondence principle, as the Heisenberg equation for the annihilation operator reads

$$\frac{d\hat{a}_j}{dt} = \frac{i}{\hbar} [\hat{\mathcal{H}}, \hat{a}_j] = -i\omega_j \hat{a}_j. \quad (13)$$

The form of both modes at  $t < 0$  and the Hamiltonian in Eq. (12) are valid for both LHTLs under consideration. The difference between the two schemes relies only on the dispersion relations and the Hamiltonian eigenenergies. The explicit form of the time-dependent eigenenergies  $\epsilon_j^{(e)}(t)$  is

$$\epsilon_j^{(1)}(t) = \hbar \sqrt{\frac{\chi_j \tilde{E}(t)}{C}}, \quad (14)$$

$$\epsilon_j^{(2)}(t) = \hbar \sqrt{\frac{\chi_j \tilde{E}(t)}{C} \sqrt{\chi_j + \frac{1}{L\tilde{E}(t)}}}. \quad (15)$$

for circuits 1 and 2, respectively.

We notice that, due to the discrepancy between eigenenergies and frequencies in LHTLs, the eigenenergies of LHTLs and RHTLs behave in a similar manner: The lower the wave vectors, the lower the eigenenergies. This is evident in Fig. 3, where we plotted both the eigenenergies and the frequencies of the massless modes of LHTL 1 and RHTL 2, and in Fig. 4, where we plotted both the eigenenergies and the frequencies of the massive modes of RHTL 1 and LHTL 2. We remind the reader that, unlike LHTLs, the eigenenergies of the Hamiltonian in RHTLs coincide with the mode frequencies  $\hat{\mathcal{H}}^R = \sum_j \epsilon_j(v_j)(\hat{b}_j^\dagger \hat{b}_j + \frac{1}{2}) \equiv \sum_j \hbar v_j (\hat{b}_j^\dagger \hat{b}_j + \frac{1}{2})$ , where the right-handed frequencies are given in Eq. (A1) for the right-handed circuit 1 in Fig. 2(b) and in Eq. (A2) for the right-handed circuit 2 in Fig. 2(c).

Before concluding this section, we want to stress that the discrepancy between eigenenergies and frequencies in LHTLs has relevant consequences on the dynamics of the ladder operators. Indeed, the Heisenberg equation in Eq. (13) demonstrates that the time evolution of the ladder operators strictly depends on the mode frequencies. Therefore, due to

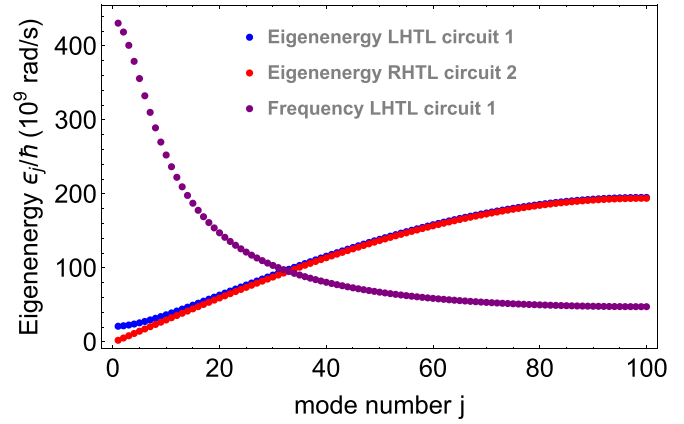


FIG. 3. Eigenenergies and dispersion relation of the transmission line showing a massless dispersion relation. Plots refer to Hamiltonian eigenenergies of the left-handed circuit 1 (red) and the right-handed circuit 2 (blue), as well as the dispersion relations of the left-handed circuit 1 (purple). Parameters are  $C = 0.4$  pF,  $L = 60$  pH,  $C_j = 0.02$  pF,  $I_c = 1.25$   $\mu$ A, and  $N = 200$ .

the commutation relation in Eq. (11), the higher the mode frequency, the lower the energy required to excite it. Crucially, this quantum feature of LHTLs also plays a decisive role, for example, in the description of resonant interactions between bosonic modes or in particle creation phenomena, as we will see in the next section.

#### IV. PARTICLE CREATION

The time-dependent Josephson energy acts as an external drive in the dynamics of the TLs. When the modulation frequency  $\Omega$  is of the same order of magnitude of the TL mode frequencies, particle creation phenomena can occur due to the presence of a resonance [2]. To describe such phenomena, we need to solve the equation of motion with respect to the magnetic flux field modes, or in other words, we need to find

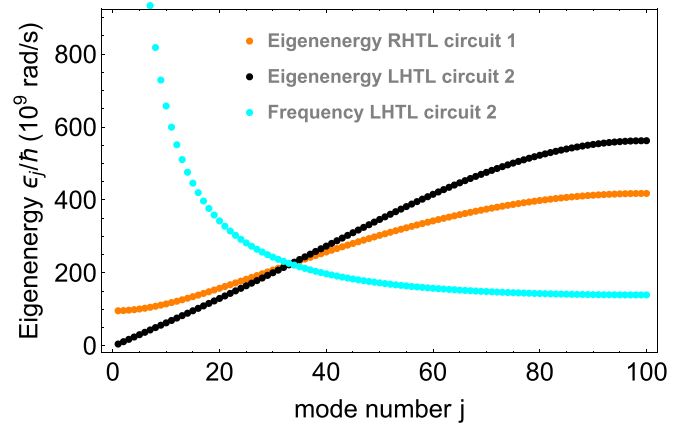


FIG. 4. Eigenenergies and dispersion relation of the transmission line showing a massive dispersion relation. Plots refer to Hamiltonian eigenenergies of the right-handed circuit 1 (orange) and the left-handed circuit 2 (black), as well as the dispersion relations of the left-handed circuit 1 (cyan). Parameters are  $C = 0.4$  pF,  $L = 60$  pH,  $C_j = 0.02$  pF,  $I_c = 1.25$   $\mu$ A, and  $N = 200$ .

the relation between the annihilation and creation operators of the magnetic flux modes before the beginning of the dynamics (input operators) and the ladder operators obtained once the modulation of the Josephson energy ceases (output operators). Since the Hamiltonian describes linear dynamics for small modulations of the Josephson energy, the input and output ladder operators are related by *Bogoliubov transformations* [2–4], which have the generic form:

$$\hat{a}_i^{\text{out}} = \sum_{|j|=1}^{N/2} (\alpha_{ji} \hat{a}_j^{\text{in}} + \beta_{ji}^* \hat{a}_j^{\dagger \text{in}}), \quad (16)$$

where the explicit expression of the coefficients  $\alpha_{ij}$  and  $\beta_{ij}$  depend on the specific TL. A more detailed description of the input-output formalism, as well as the solution of the equations of motion achieved by means of multiscale analysis [8,56], is reported in Appendixes B and C.

The phenomenon of particle creation is strongly connected to the coefficients  $\beta_{ij}$  in Eq. (16). Indeed, when these coefficients are nonzero, the initial vacuum state of the quantum field does not correspond to the quantum vacuum at the end of the dynamics, and the output operators in Eq. (16) do not act as annihilation operators of the initial quantum vacuum [2].

In the TLs under consideration, when the modulation frequency of the Josephson energy is exactly twice the frequency of one of the TL modes  $\Omega = 2\omega_h$ , the coefficient  $\beta_{hh}^*$  in Eq. (16) does not vanish, and the operator  $\hat{a}_h^{\text{out}}$  acts on the input state as a squeezed annihilation operator. If the system is initially prepared in the vacuum state  $|0\rangle = |0_{-N/2}, \dots, 0_{-1}, 0_1, \dots, 0_{N/2}\rangle$ , we can estimate the average number of particles in the resonant mode  $\omega_h$  created during the squeezing process as the expectation value of the output number operator  $\hat{N}_h = (\hat{a}_h^{\text{out}})^\dagger \hat{a}_h^{\text{out}}$ . Therefore, the output number of particles  $\langle \hat{N}_h(\tau) \rangle$  and the average energy  $\langle \hat{H}(\tau) \rangle$  at time  $\tau = \eta t$  are respectively given by  $N_h(\tau) = \sum_j |\beta_{jh}(\tau)|^2 = |\beta_{hh}(\tau)|^2$  and  $E_h(\tau) = \epsilon_h N_h(\tau)$ .

Before studying these quantities numerically, we first notice that the analytical expression for the output photon number  $N_h(\tau)$  does not depend on the left- or right-handedness of the TL, but it only depends on the massive or massless character of the Josephson energy in the dispersion relation (see Appendix C). The number of particles created is given by

$$N_h(\tau) = \sinh^2(\kappa_h \tau), \quad (17a)$$

$$N_h(\tau) = \sinh^2\left(\frac{\tilde{E}_0 \tau}{C \kappa_h}\right), \quad (17b)$$

for the massless and massive cases, respectively, with  $\kappa = \omega, \nu$ . We notice that, although Eq. (17a) is formally identical to the number of photons created via DCE in a cavity confining a quantum scalar field [5], the wave vector of the TLs is not time dependent; therefore, the Josephson energy does not simulate the modulation of the cavity length [57,58]. We can provide a more accurate physical interpretation by analyzing the modes in the proximity of the infrared limit  $\omega_j \simeq \omega_{\text{IR}}$ . Indeed, in this limit, the TL can simulate scenarios wherein the time dependence of the Josephson energy mimics the modulation of the speed of light [34,59].

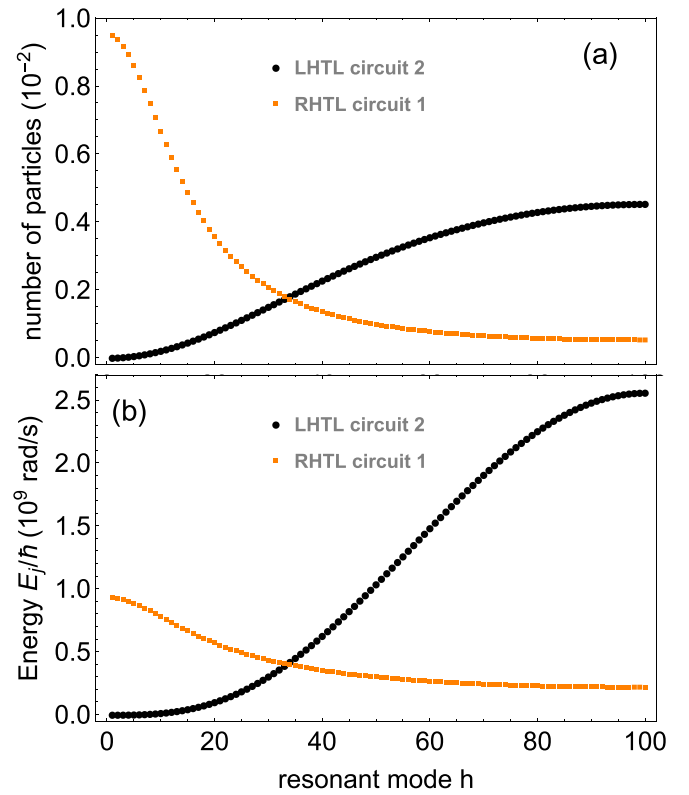


FIG. 5. (a) Expected population of massive excitations and (b) relative average energy at time  $\tau$  of the mode  $h$  by activating the resonance condition  $\Omega = 2\omega_h$  in the left-handed transmission line (LHTL) and  $\Omega = 2\nu_h$  in the right-handed transmission line (RHTL). Plots refer to left-handed circuit 2 (black) and right-handed circuit 1 (orange). Parameters are  $C = 0.4$  pF,  $L = 60$  pH,  $C_j = 0.02$  pF,  $I_c = 1.25$   $\mu$ A,  $N = 200$ , and  $\tau = 1$  ps.

The result in Eq. (17b) can be interpreted through the lens of quantum field theory as the creation of particles due to the modulation of the mass of the quantum field. In right-handed quantum fields, the time modulation of the massive term can be associated to the time dependence of the metric describing the structure of the space-time [2,32,33]. In case of the LHTL in circuit 2, Eq. (3) does not correspond to the Lagrangian of a Klein-Gordon scalar field, and the investigation of gravitational effects on quantum fields with left-handed dispersion relation would require a more comprehensive analysis that is beyond the scope of this paper.

We now want to study the behavior of  $N_h(\tau)$  and  $E_h(\tau)$  in the two LHTLs depicted in Figs. 1(b) and 1(c) as well as in the two RHTLs in Figs. 2(b) and 2(c). Results of our investigation are plotted in Figs. 5 and 6. In these graphs, each value represents the expected particle number and the energy of the mode  $h$  at time  $\tau$ , assuming that this mode is resonant with the Josephson energy of the SQUID via the resonance condition  $\Omega = 2\omega_h$  (or  $\Omega = 2\nu_h$  in the case of RHTLs).

### A. Creation of massive particles

We first discuss the particle creation in the two devices characterized by a massive dispersion relation, namely,

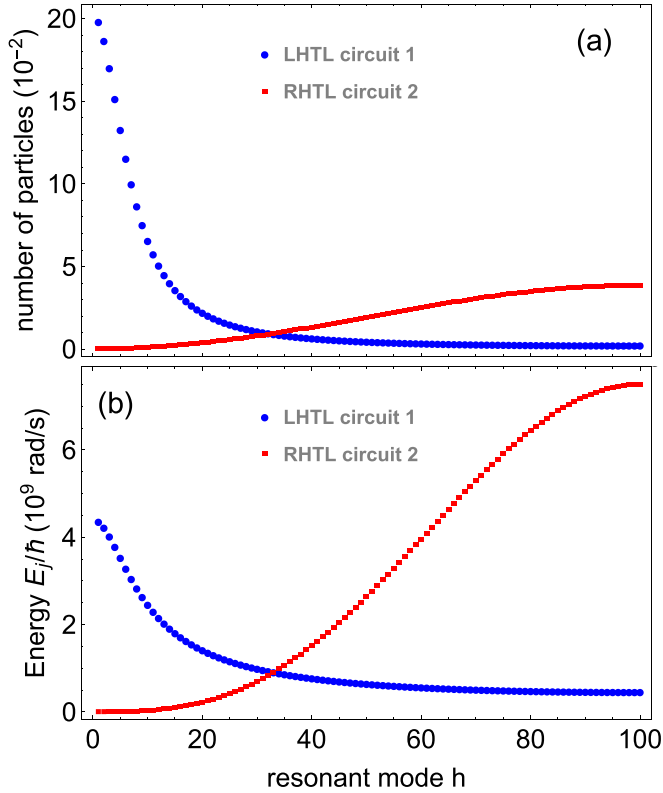


FIG. 6. (a) Expected population of massless excitations and (b) relative average energy at time  $\tau$  of the mode  $h$  by activating the resonance condition  $\Omega = 2\omega_h$  in the left-handed transmission line (LHTL) and  $\Omega = 2\nu_h$  in the right-handed transmission line (RHTL). Plots refer to left-handed circuit 1 (blue) and right-handed circuit 2 (red). With the same set of circuit parameters in all LHTLs and RHTLs, the use of our left-handed circuit 1 leads to the creation of the highest number of particles among the platforms under consideration (see also Fig. 5). Parameters are  $C = 0.4$  pF,  $L = 60$  pH,  $C_j = 0.02$  pF,  $I_c = 1.25$   $\mu$ A,  $N = 200$ , and  $\tau = 1$  ps.

left-handed circuit 2 and right-handed circuit 1. The graph in Fig. 5(a) shows that the LHTL generates a greater number of massive particles at higher mode number, whereas the RHTL favors particle creation in long-wavelength modes.

The comparison between the number of particles in Fig. 5(a) and the average energy in Fig. 5(b) demonstrates that, at the peak of the photon number curves, the maximum of the output average energy is higher in the LHTL than in the RHTL. This suggests that the creation of massive particles results energetically more convenient in right-handed circuit 1 (orange curve) than in left-handed circuit 2 (black curve).

We also notice that the creation of particles in the LHTL is drastically suppressed in modes having low mode number, namely, those modes characterized by low eigenenergies but high frequencies. The suppression of the particle creation despite the activation of the resonant condition can be exploited for the implementation of quasiadiabatic high-frequency resonant processes. Such processes can be of interest, for instance, in quantum thermodynamics, particularly in the study of adiabatic phenomena characterized by inner friction [60].

## B. Creation of massless particles

The graph in Fig. 6(a) shows the different trends of the particle creation in LHTL and RHTL having a massless dispersion relation. We observe that the resonant mode  $\nu_h$  of the RHTL emits on average more particles at higher mode numbers (red dots), while in LHTL, the number of massless particles in the resonant mode  $\omega_h$  drastically increases at lower mode numbers (blue dots). This is due to the fact that the number of output particles  $N_h(\tau)$  in Eq. (17a) increases with the mode frequency and not with the mode eigenenergy.

We remind the reader that the number of particles generated via resonant processes in the RHTL increases with the frequency/energy of the mode. However, this has two important consequences: On the one hand, the creation of low-frequency particles leads to the creation of few particles. On the other hand, the creation of high-frequency particles would require the resonant stimulation of a highly energetic mode, with the inevitable enhancement of the energy cost.

The blue dotted curve in Fig. 6(a) shows that, with the same set of circuit parameters, left-handed circuit 1 permits the creation of the highest amount of particles among the platforms analyzed in this paper [see also Fig. 6(a)], paying a reduced energy cost with respect to right-handed circuit 2, which also generates massless bosons. This becomes clearer in Fig. 6(b), where we plotted the average of the output energy with respect to the resonant mode assuming the usual resonance conditions. Despite both the higher frequency and the higher number of created particles, the energy cost of the particle creation results are lower in the LHTL than in the RHTL. This is evident from the fact that the peak of the blue dotted line in Fig. 6(b) is lower than the peak of red curve. This demonstrates that platforms based on LHTLs drastically facilitate the investigation of particle creation, making this phenomenon more accessible experimentally. Furthermore, beyond further theoretical speculations, these results suggest that the LHTL in Fig. 1(b) can find useful applications, for example, in the resonant amplifications of standard (right-handed) low-energetic signals.

## V. CONCLUSIONS

In this paper, we aimed at quantizing left-handed metamaterial TLs and studying their quantum dynamics. We used quantum field theory to quantize the magnetic flux field in LHTLs, providing the commutation rules for the ladder operators and demonstrating the presence of a discrepancy between frequencies and eigenenergies. In this framework, we then investigated the creation of particles due to resonant modulation of the Josephson energies and compared the number of particles generated in LHTLs and RHTLs.

Our results demonstrate not only that particle production in RHTLs and LHTLs shows strong mathematical similarities but also that, due to the peculiar dispersion relation in LHTLs, this phenomenon is drastically amplified in LHTLs for low-energetic massless modes. The amplification of particle creation at lower energies allows for an easier experimental accessibility to the phenomenon, which can in turn provide several concrete advantages. For these reasons, we believe that these platforms could find interesting applications in

quantum technologies, such as sensing and amplification of low-frequency signals. This paper also paves the way to future investigations of quantum field simulators based on left-handed metamaterial TLs.

### ACKNOWLEDGMENTS

A.F. thanks Göran Johansson for the useful comments. A.F., D.E.B., and F.K.W. acknowledge support from the joint Project No. 13N15685 “German Quantum Computer based on Superconducting Qubits (GeQCoS)” sponsored by the German Federal Ministry of Education and Research (BMBF) under the framework programme “Quantum technologies—from basic research to the market”. D.E.B. also acknowledges support from BMBF via the framework programme “Quantum technologies—from basic research to the market” under Contract No. 13N16210 “SPINNING”.

### APPENDIX A: RHTLS

In this section, we want to make a comparison between our two LHTLs and the equivalent RHTLs illustrated in Figs. 2(b) and 2(c). The first scheme we want to consider, which we have named right-handed circuit 1, is represented in Fig. 2(b), and it is achieved from the standard RHTL in Fig. 2(a) by replacing all capacitors with SQUIDs. A similar circuit was already proposed as an analog of a scalar field interacting with the the gravitational field [33]. The dispersion relation of such an RHTL is

$$v_j(t) = \sqrt{\frac{4 \sin^2\left(\frac{p_j \Delta x}{2}\right)}{LC} + \frac{\tilde{E}(t)}{C}}, \quad (\text{A1})$$

with  $C \equiv C_j$ . In this paper,  $v_j$  and  $p_j$  always indicate the frequency and the wave vector in the RHTL, respectively. In the framework of quantum field theory, this expression suggests that the second term inside the square root is related to the presence of a massive term with mass parameter  $M^2(t) \propto \tilde{E}(t)/C$ , see Ref. [39].

The second RHTL, which we refer to as right-handed circuit 2, is illustrated in Fig. 2(c) and is implemented from the scheme in Fig. 2(a) by replacing all inductors with a set of SQUIDs [61]. A similar scheme was realized for the study of nonlinear effects in the bare frequencies of the Hamiltonian (Kerr effect) [54]. The dispersion relation in this TL reads

$$\begin{aligned} v_j(t) &= 2 \sin\left(\frac{p_j \Delta x}{2}\right) \sqrt{\frac{\tilde{E}(t)}{C + 4C_j \sin^2\left(\frac{p_j \Delta x}{2}\right)}} \\ &\simeq 2 \sin\left(\frac{p_j \Delta x}{2}\right) \sqrt{\frac{\tilde{E}(t)}{C}}, \end{aligned} \quad (\text{A2})$$

where we assumed  $4C_j \ll C$ .

The Hamiltonian of RHTLs under consideration takes the same form for both schemes in Figs. 2(b) and 2(c), namely,

$$\hat{H}_R = \hbar \sum_{|j|=1}^{N/2} v_j \hat{b}_j^\dagger \hat{b}_j. \quad (\text{A3})$$

A direct comparison between the dispersion relations in LHTLs [see Eqs. (2) and (4) in the main text] and in RHTLs [see Eqs. (A1) and (A2)] shows interesting analogies. For instance, the Josephson energy can play the role of a massless or massive term in both types of TLs. Finally, the fact that the dispersion relation of left-handed circuit 1 shares the same form of the dispersion relation of right-handed circuit 2, and analogously for the other two schemes, is a further signature of the duality between LHTLs and RHTLs.

### APPENDIX B: DYNAMICS AND BOGOLIUBOV TRANSFORMATION

To study the dynamics at  $t > 0$ , we use the procedure employed in Refs. [8,56]. Arguments presented in this section are valid for both LHTLs considered in this paper. When the modulation of the Josephson energy starts, each mode can be written as

$$\phi_j(n, t > 0) = \sum_{|l|=1}^{N/2} \sqrt{\frac{\hbar}{CN}} Q_{jl}(t) \exp(ik_l n \Delta x), \quad (\text{B1})$$

where  $Q_{jl}(t)$ 's are solutions of the equations of motion with continuity conditions  $Q_{jl}(0) = \delta_{jl}/\sqrt{2\omega_{0j}}$  and  $\dot{Q}_{jl}(0) = -i\delta_{jl}\sqrt{2\omega_{0j}}$ , with  $\omega_{0j} \equiv \omega_j(t \leq 0)$ .

The explicit expressions for  $Q_{jl}(t)$  are achieved by solving the equations of motion. The substitution of Eq. (B1) into the equations of motion yields

$$\sum_{|l|=1}^{N/2} \left[ \frac{\ddot{Q}_{jl}(t)}{\omega_j^2(t)} + Q_{jl}(t) \right] \exp(in \Delta x k_l) = 0. \quad (\text{B2})$$

Multiplying both sides of the equation by  $\exp(-in \Delta x k_h)/N$ , summing over  $n$ , and exploiting the representation of the Kronecker delta provided before, we obtain

$$\ddot{Q}_{jh}(t) + \omega_h^2(t) Q_{jh}(t) = 0. \quad (\text{B3})$$

To solve it, we employ the multiple scale analysis. Details about this strategy as well as the solutions of this equation are reported in the next section. Once the Josephson energy returns to its original value at time  $t_f$ ,  $E(t_f) = E(0) \equiv E_0$ , and remains constant, the solution of the equation of motion simply becomes

$$Q_{jh} = A_{jh} \exp(i\omega_{0h} t) + B_{jh} \exp(-i\omega_{0h} t), \quad (\text{B4})$$

where the coefficients  $A_{jh}$  and  $B_{jh}$  are determined by the continuity condition of each  $Q_{jh}$  at the end of the motion. The explicit form of the coefficients  $A_{jh}$  and  $B_{jh}$  is calculated for the two LHTLs in the next section.

Note that the *input* and *output* modes determine the quantum vacuum at different times, and their relation is described by Bogoliubov transformations in Eq. (16). Substituting Eq. (B4) into Eq. (B1), we achieve the form of output Fourier mode expansion of the field with respect to the input modes. Recombining all terms properly and comparing with respect to Eq. (16), we observe that

$$\begin{aligned} \alpha_{jh} &= \sqrt{2\omega_{0h}} B_{jh}, \\ \beta_{jh} &= \sqrt{2\omega_{0h}} A_{jh}. \end{aligned} \quad (\text{B5})$$

These formulas relate both Bogoliubov coefficients to the coefficients  $A_{jh}$  and  $B_{jh}$ .

### APPENDIX C: MULTIPLE SCALE ANALYSIS

In this section, we present the solution strategy to solve Eq. (B3) for the two LHTLs. This formalism is presented in Ref. [56]. As first, we define a new time scale  $\tau = \eta t$  and expand  $Q_{jh}(t)$  with respect to  $\eta$ :

$$\begin{aligned} Q_{jh}(t) &= Q_{jh}^{(0)}(t, \tau) + \eta Q_{jh}^{(1)}(t, \tau), \\ \ddot{Q}_{jh}(t) &= \partial_t^2 Q_{jh}^{(0)}(t, \tau) + \eta \left[ 2\partial_{\tau t}^2 Q_{jh}^{(0)}(t, \tau) + \partial_t^2 Q_{jh}^{(1)}(t, \tau) \right], \end{aligned} \quad (\text{C1})$$

where  $\partial_t^2 \equiv \partial^2/\partial t^2$  and  $\partial_{\tau t}^2 \equiv \partial^2/(\partial\tau\partial t)$ . We now substitute Eq. (C1) into Eq. (B3) and solve this equation at different

orders in  $\tau$ . At the zeroth order in  $\tau$ , we simply achieve

$$\ddot{Q}_{jh}^{(0)} + \omega_{h0}^2 Q_{jh}^{(0)} = 0, \quad (\text{C2})$$

whose solution is

$$Q_{jh}^{(0)}(t, \tau) = A_{jh}(\tau) \exp(i\omega_{h0}t) + B_{jh}(\tau) \exp(-i\omega_{h0}t). \quad (\text{C3})$$

From the continuity conditions for  $Q_{jh}(t)$ , we have the following initial conditions for  $A_{jh}(\tau)$  and  $B_{jh}(\tau)$ :

$$\begin{aligned} A_{jh}(0) &= 0, \\ B_{jh}(0) &= \frac{1}{\sqrt{2\omega_{h0}}} \delta_{jh}. \end{aligned} \quad (\text{C4})$$

We now focus on circuit 1, describing a quantum magnetic flux field with massless excitations and dispersion relation given in Eq. (2) of the main text. Considering only the first order in  $\tau$ , Eq. (B3) becomes

$$2\partial_{\tau t} Q_{jh}^{(0)} + \partial_t^2 Q_{jh}^{(1)} + \omega_{h0}^2 Q_{jh}^{(1)} + 4\omega_{h0}^2 \sin(\Omega t) Q_{jh}^{(0)} = 0. \quad (\text{C5})$$

Substituting the solution of the zeroth order, Eq. (C3), into Eq. (C5), we obtain

$$\begin{aligned} \partial_t^2 Q_{jh}^{(1)} + \omega_{h0}^2 Q_{jh}^{(1)} &= -2\partial_{\tau t} Q_{jh}^{(0)} - 4\omega_{h0}^2 \sin(\Omega t) Q_{jh}^{(0)} \\ &= -2i\omega_{h0} \left[ (\partial_{\tau} A_{jh}) \exp(i\omega_{h0}t) - (\partial_{\tau} B_{jh}) \exp(-i\omega_{h0}t) \right] \\ &\quad + 2i\omega_{h0}^2 [\exp(i\Omega t) - \exp(-i\Omega t)] [A_{jh} \exp(i\omega_{h0}t) + B_{jh} \exp(-i\omega_{h0}t)] \\ &= -2i\omega_{h0} \exp(i\omega_{h0}t) \{ (\partial_{\tau} A_{jh}) - \omega_{h0} B_{jh} \exp[i(\Omega - 2\omega_{h0})t] \} \\ &\quad + 2i\omega_{h0} \exp(-i\omega_{h0}t) \{ (\partial_{\tau} B_{jh}) - \omega_{h0} A_{jh} \exp[-i(\Omega - 2\omega_{h0})t] \}. \end{aligned} \quad (\text{C6})$$

We now seek a solution of such an equation without secularities. *Secularities* are all those terms proportional to  $\exp(\pm i\omega_{h0}t)$ , namely, all those term that are already solutions of the homogeneous equation. To avoid such secularities, we need the coefficients of  $\exp(\pm i\omega_{h0}t)$  to vanish, thereby obtaining the following set of differential equations:

$$\begin{cases} \frac{\partial A_{jh}}{\partial \tau} - \omega_{h0} \delta(\Omega - 2\omega_{h0}) B_{jh} = 0, \\ \frac{\partial B_{jh}}{\partial \tau} - \omega_{h0} \delta(\Omega - 2\omega_{h0}) A_{jh} = 0, \end{cases} \quad \text{or} \quad \begin{cases} \frac{\partial A_{jh}}{\partial \tau} = \omega_{h0} \delta(\Omega - 2\omega_{h0}) B_{jh}, \\ \frac{\partial B_{jh}}{\partial \tau} = \omega_{h0} \delta(\Omega - 2\omega_{h0}) A_{jh}. \end{cases} \quad (\text{C7})$$

These sets of equations are solved by differentiating one, substituting it into the other one, and exploiting the initial conditions in Eq. (C4). Finally, we obtain

$$\begin{aligned} A_{jh} &= \frac{1}{\sqrt{2\omega_{h0}}} \sinh(\omega_{h0}\tau) \delta_{jh} \delta(\Omega - 2\omega_{h0}), \\ B_{jh} &= \frac{1}{\sqrt{2\omega_{h0}}} \cosh(\omega_{h0}\tau) \delta_{jh} \delta(\Omega - 2\omega_{h0}). \end{aligned} \quad (\text{C8})$$

We proceed similarly for circuit 2, describing a quantum field with massive excitations. At the zeroth order in  $\tau$ , the equation for  $Q_{jh}$  is identical to Eq. (C2), where now  $\omega_{h0}$  corresponds to Eq. (4) of the main text at  $t = 0$ . At the first order, the equation is

$$2\partial_{\tau t} Q_{jh}^{(0)} + \partial_t^2 Q_{jh}^{(1)} + \omega_{h0}^2 Q_{jh}^{(1)} + \frac{4E_0}{C} \sin(\Omega t) Q_{jh}^{(0)} = 0. \quad (\text{C9})$$

Moving the zeroth order to the right side and replacing the solution of the zeroth order, Eq. (C3), into Eq. (C9), we obtain

$$\begin{aligned} \partial_t^2 Q_{jh}^{(1)} + \omega_{h0}^2 Q_{jh}^{(1)} &= -2\partial_{\tau t} Q_{jh}^{(0)} - \frac{4\tilde{E}_0}{C} \sin(\Omega t) Q_{jh}^{(0)} \\ &= -2i\omega_{h0} \left[ (\partial_{\tau} A_{jh}) \exp(i\omega_{h0}t) - (\partial_{\tau} B_{jh}) \exp(-i\omega_{h0}t) \right] \\ &\quad + \frac{2i\tilde{E}_0}{C} [\exp(i\Omega t) - \exp(-i\Omega t)] [A_{jh} \exp(i\omega_{h0}t) + B_{jh} \exp(-i\omega_{h0}t)] \end{aligned}$$

$$\begin{aligned}
&= -2i \exp(i\omega_{h0}t) \left\{ \omega_{h0}(\partial_\tau A_{jh}) - \frac{\tilde{E}_0}{C} B_{jh} \exp[i(\Omega - 2\omega_{h0})t] \right\} \\
&\quad + 2i \exp(-i\omega_{h0}t) \left\{ \omega_{h0}(\partial_\tau B_{jh}) - \frac{\tilde{E}_0}{C} A_{jh} \exp[-i(\Omega - 2\omega_{h0})t] \right\}. \tag{C10}
\end{aligned}$$

As done above, we seek a solution without secularities, and therefore, we need to solve the pair of differential equations:

$$\frac{\partial A_{jh}}{\partial \tau} = \frac{\tilde{E}_0}{C\omega_{h0}} \delta(\Omega - 2\omega_{h0}) B_{jh}, \tag{C11}$$

$$\frac{\partial B_{jh}}{\partial \tau} = \frac{\tilde{E}_0}{C\omega_{h0}} \delta(\Omega - 2\omega_{h0}) A_{jh}, \tag{C12}$$

whose solutions are

$$\begin{aligned}
A_{jh} &= \frac{1}{\sqrt{2\omega_{h0}}} \sinh\left(\frac{\tilde{E}_0 \tau}{C\omega_{h0}}\right) \delta_{jh} \delta(\Omega - 2\omega_{h0}), \\
B_{jh} &= \frac{1}{\sqrt{2\omega_{h0}}} \cosh\left(\frac{\tilde{E}_0 \tau}{C\omega_{h0}}\right) \delta_{jh} \delta(\Omega - 2\omega_{h0}). \tag{C13}
\end{aligned}$$

A crucial consequence of the duality between LHTLs and RHTLs is that, by repeating the same procedure and solving the equations of motion for RHTLs, we exactly obtain Eqs. (C8) and (C13) in the massless and massive cases, respectively (with  $\omega_{0h}$  instead of  $\omega_{h0}$ ).

- 
- [1] M. D. Schwartz, *Quantum Field Theory and the Standard Model* (Cambridge University Press, Cambridge, 2014).
- [2] N. D. Birrell and P. C. W. Davies, *Quantum Fields in Curved Space* (Cambridge University Press, Cambridge, 1984).
- [3] L. H. Ford, Cosmological particle production: A review, *Rep. Prog. Phys.* **84**, 116901 (2021).
- [4] E. Martín-Martínez and N. C. Menicucci, Entanglement in curved spacetimes and cosmology, *Class. Quantum Gravity* **31**, 214001 (2014).
- [5] V. Dodonov, Fifty years of the dynamical Casimir effect, *Physics* **2**, 67 (2009).
- [6] C. K. Law, Resonance response of the quantum vacuum to an oscillating boundary, *Phys. Rev. Lett.* **73**, 1931 (1994).
- [7] V. V. Dodonov and A. B. Klimov, Generation and detection of photons in a cavity with a resonantly oscillating boundary, *Phys. Rev. A* **53**, 2664 (1996).
- [8] M. Crocce, D. A. R. Dalvit, and F. D. Mazzitelli, Resonant photon creation in a three-dimensional oscillating cavity, *Phys. Rev. A* **64**, 013808 (2001).
- [9] W. G. Unruh, Notes on black-hole evaporation, *Phys. Rev. D* **14**, 870 (1976).
- [10] L. C. B. Crispino, A. Higuchi, and G. E. A. Matsas, The Unruh effect and its applications, *Rev. Mod. Phys.* **80**, 787 (2008).
- [11] C. J. Fewster, B. A. Juárez-Aubry, and J. Louko, Waiting for Unruh, *Class. Quantum Grav.* **33**, 165003 (2016).
- [12] D. E. Bruschi, J. Louko, E. Martín-Martínez, A. Dragan, and I. Fuentes, Unruh effect in quantum information beyond the single-mode approximation, *Phys. Rev. A* **82**, 042332 (2010).
- [13] S. W. Hawking, Black hole explosions? *Nature (London)* **248**, 30 (1974).
- [14] M. K. Parikh and F. Wilczek, Hawking radiation as tunneling, *Phys. Rev. Lett.* **85**, 5042 (2000).
- [15] A. Almheiri, T. Hartman, J. Maldacena, E. Shaghoulian, and A. Tajdini, The entropy of Hawking radiation, *Rev. Mod. Phys.* **93**, 035002 (2021).
- [16] C. M. Wilson, T. Duty, M. Sandberg, F. Persson, V. Shumeiko, and P. Delsing, Photon generation in an electromagnetic cavity with a time-dependent boundary, *Phys. Rev. Lett.* **105**, 233907 (2010).
- [17] C. M. Wilson, G. Johansson, A. Pourkabirian, M. Simoen, J. R. Johansson, T. Duty, F. Nori, and P. Delsing, Observation of the dynamical Casimir effect in a superconducting circuit, *Nature (London)* **479**, 376 (2011).
- [18] J. Steinhauer, Observation of quantum Hawking radiation and its entanglement in an analogue black hole, *Nat. Phys.* **12**, 959 (2016).
- [19] P. O. Fedichev and U. R. Fischer, ‘‘Cosmological’’ quasiparticle production in harmonically trapped superfluid gases, *Phys. Rev. A* **69**, 033602 (2004).
- [20] J. R. Muñoz De Nova, K. Golubkov, V. I. Kolobov, and J. Steinhauer, Observation of thermal Hawking radiation and its temperature in an analogue black hole, *Nature (London)* **569**, 688 (2019).
- [21] Y.-H. Shi, R.-Q. Yang, Z. Xiang, Z.-Y. Ge, H. Li, Y.-Y. Wang, K. Huang, Y. Tian, X. Song, D. Zheng *et al.*, Quantum simulation of Hawking radiation and curved spacetime with a superconducting on-chip black hole, *Nat. Commun.* **14**, 3263 (2023).
- [22] I. M. Georgescu, S. Ashhab, and F. Nori, Quantum simulation, *Rev. Mod. Phys.* **86**, 153 (2014).
- [23] J. Q. You and F. Nori, Atomic physics and quantum optics using superconducting circuits, *Nature (London)* **474**, 589 (2011).
- [24] B. Yurke and J. S. Denker, Quantum network theory, *Phys. Rev. A* **29**, 1419 (1984).
- [25] A. Blais, R.-S. Huang, A. Wallraff, S. M. Girvin, and R. J. Schoelkopf, Cavity quantum electrodynamics for superconducting electrical circuits: An architecture for quantum computation, *Phys. Rev. A* **69**, 062320 (2004).
- [26] A. Blais, A. L. Grimsmo, S. M. Girvin, and A. Wallraff, Circuit quantum electrodynamics, *Rev. Mod. Phys.* **93**, 025005 (2021).

- [27] J. Zhang, R. Ferguson, S. Kühn, J. F. Haase, C. Wilson, K. Jansen, and C. A. Muschik, Simulating gauge theories with variational quantum eigensolvers in superconducting microwave cavities, *Quantum* **7**, 1148 (2023).
- [28] D. M. Pozar, *Microwave Engineering* (John Wiley & Sons, Hoboken, 2011).
- [29] U. Vool and M. Devoret, Introduction to quantum electromagnetic circuits, *Int. J. Circuit Theory Appl.* **45**, 897 (2017).
- [30] C. Sabín, Analogue non-causal null curves and chronology protection in a dc-SQUID array, *Universe* **8**, 452 (2022).
- [31] A. Terrones and C. Sabín, Towards quantum simulation of black holes in a dc-SQUID array, *Universe* **7**, 499 (2021).
- [32] P. D. Nation, J. R. Johansson, M. P. Blencowe, and F. Nori, *Colloquium*: Stimulating uncertainty: Amplifying the quantum vacuum with superconducting circuits, *Rev. Mod. Phys.* **84**, 1 (2012).
- [33] Z. Tian, J. Jing, and A. Dragan, Analog cosmological particle generation in a superconducting circuit, *Phys. Rev. D* **95**, 125003 (2017).
- [34] S. Lang and R. Schützhold, Analog of cosmological particle creation in electromagnetic waveguides, *Phys. Rev. D* **100**, 065003 (2019).
- [35] P. Lähteenmäki, G. S. Paraoanu, J. Hassel, and P. J. Hakonen, Dynamical Casimir effect in a Josephson metamaterial, *Proc. Natl. Acad. Sci.* **110**, 4234 (2013).
- [36] J. R. Johansson, G. Johansson, C. M. Wilson, and F. Nori, Dynamical Casimir effect in a superconducting coplanar waveguide, *Phys. Rev. Lett.* **103**, 147003 (2009).
- [37] J. R. Johansson, G. Johansson, C. M. Wilson, and F. Nori, Dynamical Casimir effect in superconducting microwave circuits, *Phys. Rev. A* **82**, 052509 (2010).
- [38] P. D. Nation, M. P. Blencowe, A. J. Rimberg, and E. Buks, Analogue Hawking radiation in a dc-SQUID array transmission line, *Phys. Rev. Lett.* **103**, 087004 (2009).
- [39] Z. Tian and J. Du, Analogue Hawking radiation and quantum soliton evaporation in a superconducting circuit, *Eur. Phys. J. C* **79**, 994 (2019).
- [40] M. P. Blencowe and H. Wang, Analogue gravity on a superconducting chip, *Philos. Trans. R. Soc. A* **378**, 20190224 (2020).
- [41] D. R. Smith, W. J. Padilla, D. C. Vier, S. C. Nemat-Nasser, and S. Schultz, Composite medium with simultaneously negative permeability and permittivity, *Phys. Rev. Lett.* **84**, 4184 (2000).
- [42] D. R. Smith and N. Kroll, Negative refractive index in left-handed materials, *Phys. Rev. Lett.* **85**, 2933 (2000).
- [43] A. A. Houck, J. B. Brock, and I. L. Chuang, Experimental observations of a left-handed material that obeys Snell's law, *Phys. Rev. Lett.* **90**, 137401 (2003).
- [44] V. G. Veselago, Electrodynamics of substances with simultaneously negative and, *Usp. Fiz. Nauk.* **92**, 517 (1967).
- [45] A. B. Kozyrev and D. W. Van Der Weide, Nonlinear left-handed transmission line metamaterials, *J. Phys. D* **41**, 173001 (2008).
- [46] A. Alizadeh, B. Rejaei, and M. Fardmanesh, Tunable stopband HTS Josephson junction left-handed transmission line with independently biasable unit cells, *IEEE Trans. Appl. Supercond.* **30**, 1500108 (2020).
- [47] D. J. Egger and F. K. Wilhelm, Multimode circuit quantum electrodynamics with hybrid metamaterial transmission lines, *Phys. Rev. Lett.* **111**, 163601 (2013).
- [48] A. Messinger, B. G. Taketani, and F. K. Wilhelm, Left-handed superlattice metamaterials for circuit QED, *Phys. Rev. A* **99**, 032325 (2019).
- [49] H. Wang, A. P. Zhuravel, S. Indrajeet, B. G. Taketani, M. D. Hutchings, Y. Hao, F. Rouxinol, F. K. Wilhelm, M. D. LaHaye, A. V. Ustinov *et al.*, Mode structure in superconducting metamaterial transmission-line resonators, *Phys. Rev. Appl.* **11**, 054062 (2019).
- [50] S. Indrajeet, H. Wang, M. D. Hutchings, B. G. Taketani, F. K. Wilhelm, M. D. LaHaye, and B. L. T. Plourde, Coupling a superconducting qubit to a left-handed metamaterial resonator, *Phys. Rev. Appl.* **14**, 064033 (2020).
- [51] T. McBroom-Carroll, A. Schlabe, X. Xu, J. Ku, B. Cole, S. Indrajeet, M. D. LaHaye, M. H. Ansari, and B. L. T. Plourde, Entangling interactions between artificial atoms mediated by a multimode left-handed superconducting ring resonator, *PRX Quantum* **5**, 020325 (2024).
- [52] E. A. Ovchinnikova, S. Butz, P. Jung, V. P. Koshelets, L. V. Filippenko, A. S. Averkin, S. V. Shitov, and A. V. Ustinov, Design and experimental study of superconducting left-handed transmission lines with tunable dispersion, *Supercond. Sci. Technol.* **26**, 114003 (2013).
- [53] O. V. Shramkova, N. Lazarides, G. P. Tsironis, and A. V. Ustinov, Electrically and magnetically resonant dc-SQUID metamaterials, *Appl. Phys. A* **123**, 58 (2017).
- [54] T. Weißl, B. Küng, E. Dumur, A. K. Feofanov, I. Matei, C. Naud, O. Buisson, F. W. J. Hekking, and W. Guichard, Kerr coefficients of plasma resonances in Josephson junction chains, *Phys. Rev. B* **92**, 104508 (2015).
- [55] M. Wallquist, V. S. Shumeiko, and G. Wendin, Selective coupling of superconducting charge qubits mediated by a tunable stripline cavity, *Phys. Rev. B* **74**, 224506 (2006).
- [56] C. M. Bender, S. Orszag, and S. A. Orszag, *Advanced Mathematical Methods for Scientists and Engineers I: Asymptotic Methods and Perturbation Theory*, Vol. 1 (Springer Science & Business Media, Berlin, 1999).
- [57] C. K. Law, Interaction between a moving mirror and radiation pressure: A Hamiltonian formulation, *Phys. Rev. A* **51**, 2537 (1995).
- [58] A. Ferreri, H. Pfeifer, F. K. Wilhelm, S. Hofferberth, and D. E. Bruschi, Interplay between optomechanics and the dynamical Casimir effect, *Phys. Rev. A* **106**, 033502 (2022).
- [59] C. Sabín, One-dimensional sections of exotic spacetimes with superconducting circuits, *New J. Phys.* **20**, 053028 (2018).
- [60] F. Plastina, A. Alecce, T. J. G. Apollaro, G. Falcone, G. Francica, F. Galve, N. Lo Gullo, and R. Zambrini, Irreversible work and inner friction in quantum thermodynamic processes, *Phys. Rev. Lett.* **113**, 260601 (2014).
- [61] N. A. Masluk, I. M. Pop, A. Kamal, Z. K. Mineev, and M. H. Devoret, Microwave characterization of Josephson junction arrays: Implementing a low loss superinductance, *Phys. Rev. Lett.* **109**, 137002 (2012).